water

MDPI

Article

Unravelling the Effect of Sediment Properties on As(V) and As(III) Adsorption/Desorption Processes: Implications for Groundwater Geochemistry

Sara Trotta [1,*], Gilberto Binda [1,2], Andrea Pozzi [1] and Alessandro Maria Michetti [1,3]

[1] Department of Science and High Technology, University of Insubria, 22100 Como, Italy
[2] Norwegian Institute for Water Research (NIVA), 0579 Oslo, Norway
[3] Osservatorio Vesuviano, Istituto Nazionale di Geofisica e Vulcanologia, Via Diocleziano 328, 80124 Naples, Italy
* Correspondence: strotta@uninsubria.it

Abstract

Arsenic (As) mobility in aquifer systems is mainly governed by its adsorption and desorption behaviour at the sediment-water interface, directly influencing its environmental availability and risks to water quality. This study explores the adsorption-desorption behaviour of inorganic As species through batch experiments on environmental sediments collected from three representative depths, selected to reflect local contrasting geochemical, mineralogical, and granulometric characteristics of the Como basin aquifer (Northern Italy). This setting was selected as a case study owing to its notable gradient in As concentration in groundwater: the shallow aquifers host concentrations typically below 10 µg/L, while the deep aquifer reaches concentrations of about 250 µg/L. Statistical analyses (ANOVA and simple linear regression) identified Mn- and Al-(hydr)oxide content, grain size, and mineralogy as strong predictors of As(V) retention, whereas As(III) showed no significant correlation with individual sediment properties within the tested conditions. Shallow, Mn- and Al-rich sediments exhibited higher adsorption capacity and corresponded to lower dissolved As in groundwater, while deeper, finer-grained sediments with lower oxide content coincided with elevated groundwater As concentrations. Desorption experiments indicated that As(III) dominated the released fraction, reflecting its greater mobility under variable pH and redox aquifer conditions. These results provide mechanistic insight into sediment-water interactions controlling As distribution in multilayer aquifers, supporting improved risk assessment and management of As in complex groundwater systems.

Keywords: sediment geochemistry; arsenic contamination; adsorption-desorption kinetics; sediment-water interface

Academic Editor: Yuanrong Zhu

Received: 14 July 2025
Revised: 25 August 2025
Accepted: 26 August 2025
Published: 4 September 2025

Citation: Trotta, S.; Binda, G.; Pozzi, A.; Michetti, A.M. Unravelling the Effect of Sediment Properties on As(V) and As(III) Adsorption/Desorption Processes: Implications for Groundwater Geochemistry. *Water* **2025**, *17*, 2616. https://doi.org/10.3390/w17172616

1. Introduction

Arsenic (As) contamination in the environment is a significant global concern due to its high toxicity and widespread occurrence in natural waters, particularly in groundwater [1,2]. Even in regions where As originates from geogenic sources [3], elevated concentrations in drinking water supplies can pose substantial risks to human health and ecosystems. Globally, it is in fact estimated that 140 million people consume water with As concentrations exceeding the WHO's recommended limit of 10 µg/L [4].

Building on this global context, the present study focuses on a geogenically impacted aquifer in Northern Italy, where naturally elevated As levels have been reported to exceed

safety limits by up to 20 times [5]. Notably, groundwater monitoring in the Como basin has revealed a pronounced vertical heterogeneity in As concentrations with aquifer depth: levels in the deep aquifer reach up to 250 µg/L, while concentrations in the shallow zone are typically below 10 µg/L [5]. However, to date, the mechanisms responsible for these concentrations remain unclear.

To address this knowledge gap, this study aims to comprehensively evaluate the mechanisms controlling the mobility of inorganic As, specifically As(III) and As(V), in natural aquifer sediments from the Como basin. Particular attention is given to the role of sediment physicochemical properties, including cation exchange capacity (CEC), grain size, mineralogy, geogenic element content, and organic matter, in influencing As adsorption-desorption dynamics.

Understanding these mechanisms requires a consideration of the geochemical origins of As and the fundamental processes that regulate its mobility in groundwater. Arsenic is widely distributed in the Earth's crust, usually found in minerals such as realgar (As_4S_4), orpiment (As_2S_3), arsenopyrite (FeAsS), and cobaltite (CoAsS) [3]. Natural rock weathering favours the release of As into water bodies, where it becomes of significant toxicological concern, as water serves as a primary medium for its transmission and subsequent exposure to humans and wildlife.

In the water compartment, As can be present in different species, including arsenious (H_3AsO_3) and arsenic (H_3AsO_4) acids and their deprotonated forms ($H_2AsO_3^-$, $HAsO_3^{2-}$, $H_2AsO_4^-$, and $HAsO_4^{2-}$), as well as organic arsenic compounds such as methylarsenic acid, dimethylarsinic acid, and arsine. In groundwater, the most toxic and well-characterised inorganic As species are the reduced trivalent arsenite As(III) and the oxidised pentavalent arsenate As(V), which can interconvert depending on the redox potential, temperature, and pH of the environment [6]. Arsenic mobility is further governed by adsorption-desorption processes at the solid-liquid interface, defining the likelihood of release from sediment and rocks into water. In this context, water and sediment/rock geochemical and physicochemical properties, along with biogeochemical processes (e.g., microbial activity), play a critical role in influencing As transport and bioavailability in aquatic systems [7].

In this regard, many studies have pointed out that sediment size is a key factor, confirming that the adsorption of As increases as sediment grain size decreases, with adsorption efficiency higher for clay and progressively lower values in silty and sandy solids [8,9]. Additionally, the presence of clay minerals has been shown to have a favourable influence, associated with the presence of iron (Fe-), aluminium(Al-), and manganese (Mn-) oxides/hydroxides [10,11]. Organic matter, on the other hand, has shown an antagonistic effect on As adsorption [12]. For example, Wang et al. (2006) [13] assessed that the presence of organic matter can promote As release primarily through competition for available adsorption sites, the formation of aqueous complexes, and alteration of the redox chemistry of site surfaces and metalloid species, resulting in increased As concentrations in the surrounding water medium. In addition to the physicochemical properties of sediment, significant research also delves into the chemical characteristics of aquifer waters and their impacts on As adsorption/desorption equilibria. Studies have investigated various factors such as pH, dissolved phosphate concentration, temperature, and the presence of competing ions, all of which can significantly influence the behaviour of As in aqueous solutions [14]. To better understand such a complex system, kinetic studies using pseudo-first-order and pseudo-second-order models (PFO and PSO) have also been applied [15].

Despite the extensive literature on As-sediment interactions, most studies evaluate total As uptake without distinguishing between chemical species or comparing their behaviours [16–19], thereby overlooking the different environmental fates and toxicities of As(III) and As(V). Moreover, studies frequently focus on specific or purified materials [20,21], investigating the influence of individual sediment properties under highly controlled conditions. While these approaches provide useful mechanistic insights, they fail to capture the complexity of natural, compositionally heterogeneous sediments, where multiple factors interact to influence adsorption-desorption dynamics and ultimately control As mobility.

Gaining a deeper understanding of As mobility in natural, compositionally complex sediments is essential for improving conceptual models of contaminant transport in groundwater systems. In particular, identifying the geochemical mechanisms that control the retention and release of As(III) and As(V) can enhance the accuracy of risk assessments and inform more effective monitoring and remediation strategies. Here, we hypothesise that the chemical composition of sediment, its grain size distribution and the initial speciation of As (i.e., III or V) are the key factors in defining its adsorption-desorption behaviour. Given that the Como basin serves as a drinking water source for a densely populated region and exhibits As levels far exceeding regulatory thresholds, this study contributes valuable insight into the natural controls on As fate in multilayer aquifer settings impacted by geogenic contamination.

2. Materials and Methods

2.1. Study Area and Sample Collection

The city of Como is situated at the southern end of the western branch of Lake Como in the Lombardy region of Italy [22–24]. Groundwater flow in the urban subsurface is restricted to two main aquifers: a shallow phreatic aquifer and a deeper confined aquifer. From a lithological point of view, the deeper confined aquifer is segmented into multiple lenses and layers; it is primarily composed of sandy glaciolacustrine deposits overlain by clays and silts [22]. This heterogeneity, combined with the complex sedimentary structure, offers an ideal opportunity to examine the relationships between different sediment characteristics and inorganic As adsorption-desorption processes.

To investigate this, the sediment core (Figure 1a) was systematically sampled at depths of 50, 60, and 70 m, with samples designated as S1, S2, and S3, respectively. These depths were specifically selected to represent distinct layers of the aquifer system that had previously been characterised by varying As concentrations in groundwater [5]. The sampling strategy was therefore designed to capture the vertical heterogeneity observed in As distribution (Figure 1b) and to assess whether geochemical properties of real-world sediments at these depths could help explain such variability. The selected samples thus enabled a comparative evaluation of sediments with differing physicochemical characteristics, providing valuable insights into how these differences influence As mobility within the aquifer.

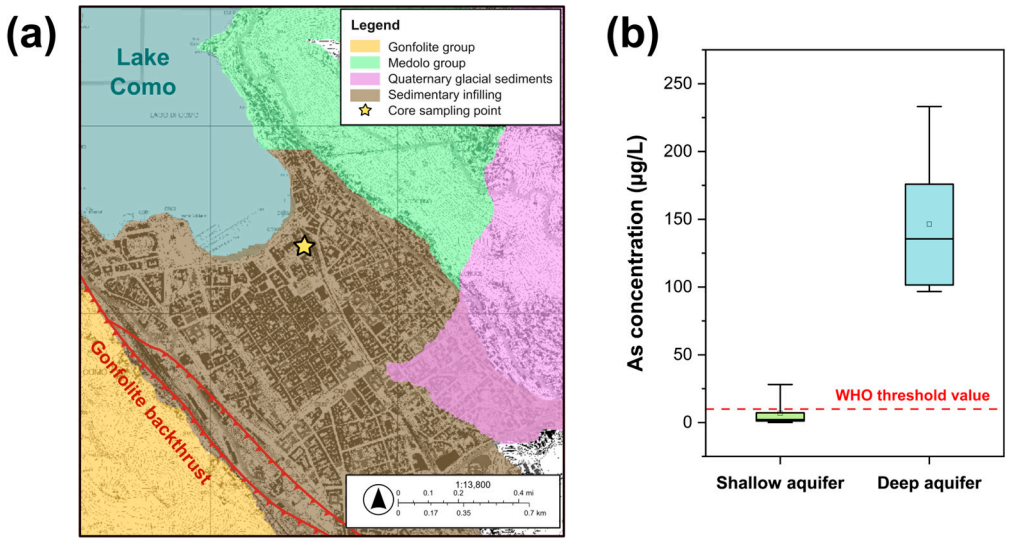

Figure 1. (**a**) Simplified geologic map of the study area (modified after [22]). The sediment sampling location is highlighted with the yellow star symbol. Topo map: CTR–Carta Tecnica Regionale, provided by Regione Lombardia (Regione Lombardia. Carta Tecnica Regionale. 1994. Available online: https://www.geoportale.regione.lombardia.it (accessed on 19 December 2024). (**b**) Box plot of As concentration in the deep aquifer (blue) and shallow aquifer (green) (modified after [5]). The boxes represent the interquartile range (25th to 75th percentile), whiskers extend to the minimum and maximum values, squares denote the mean, and horizontal lines indicate the median. The red line marks the WHO-recommended limit for As in drinking water [25].

2.2. Reagents, Materials, and Solutions

All the solutions were prepared using ultrapure water obtained from a Sartorius (Göttingen, Germany) Arium mini (18.2 MΩcm resistivity). Ultrapure HNO_3 and HCl were obtained from sub-boiling distilled nitric acid (65% *w*/*w*, Carlo Erba Reagenti, Milan, Italy) and hydrocloridric acid (37% *w*/*w*, Carlo Erba Reagenti, Milan, Italy) using a Milestone (Shelton, CT, USA) DuoPUR system [26]. As(V) stock adsorption solution was prepared by dissolving $Na_2HAsO_4{\cdot}7H_2O$ (98% wt., Carlo Erba, Milan, Italy) in ultrapure water, while As(III) stock solution was prepared by diluting a $NaAsO_3$ (Carlo Erba, Milan, Italy) standard solution. A 100 ppm As ICP-MS standard solution was used to prepare the set of standard solutions used for the instrument calibration, and an Rh standard solution (Merck, Darmstadt, Germany) was spiked into the liquid samples as an internal standard. All experiments were conducted in low-density polyethylene (LDPE, Nalgene, Rochester, NY, USA) bottles meticulously cleaned and decontaminated. This process included extended washing periods (48 h each) with a detergent solution (4 mL/L Nalgene L900) followed by rinsing with a 2% weight HNO_3 and 0.01 M HCl solution. The bottles were then rinsed three times with ultrapure water and left to air-dry under a laminar flow hood. Test tubes used for ICP-MS analysis were washed following the same protocol. Detailed analytical information and quality assurance/quality control (QA/QC) protocols are available elsewhere [27].

2.3. Sediment Characterisation

2.3.1. Grain Size Distribution

The grain size distribution (GSD) of the three sediment samples investigated was analysed using a combination of techniques outlined below. Figure 2 illustrates the methodology employed. Each sediment sample was prepared for analysis with the XL30 Environmental Scanning Electron Microscope (ESEM FEG, FEI Electron Optics International B.V., Eindhoven, The Netherlands) at 20 kV in high vacuum conditions. Samples were first dried in an oven (30 °C, 24 h), mounted onto stubs using carbon tape to ensure stability during

imaging, and consequently sputter-coated with a ~5 nm thick gold layer to enhance surface conductivity and improve image quality. A systematic imaging approach was adopted for each sediment, capturing a total of 16 images per sample, following a predefined image sampling scheme (refer to Figure 2b), ensuring representative coverage of the sample surface. The images obtained from the SEM in secondary electron mode were processed using image analysis software, specifically Fiji software, an adaptation of ImageJ (FIJI 1.46r, National Institutes of Health (NIH), Bethesda, MD, USA) [28,29]. We performed a manual statistical count of particle size for each image, and grain data were acquired as particle diameter measurements, perimeter and area. The Fiji software output was then processed using Microsoft Excel. Grain size was then calculated by measuring the Feret diameters of every grain within a one φ size class [30]. These data were utilised to compute the median grain size, denoted as D_{50} [31] and expressed in micrometres. Grain size distributions of each sample were then characterised following the standard method [32].

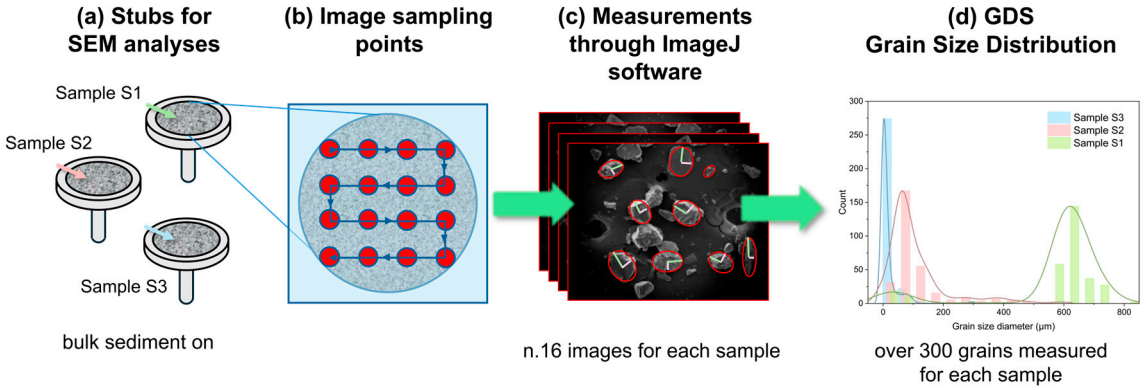

Figure 2. Schematic representation of the methodology employed to obtain the GSD data for the three samples analysed. (**a**) Preparation of the sample on the stub with bulk sediment, (**b**) sampling scheme adopted for image acquisition, (**c**) example of images taken using SEM and measurement of grain dimensions using Fiji ImageJ software, and (**d**) output of the process: an example of measurements data obtained is plotted in a distribution graph.

2.3.2. Chemistry and Mineralogy

Sediment samples underwent testing to assess physicochemical properties known to impact the adsorption of metals onto solid surfaces, as documented by previous studies [33–37]. These properties included cation exchange capacity (CEC), pH, organic content (OM%), and mineralogical composition. Before analysis, impurities were manually removed from the samples. Notably, unlike several other studies, the sediment was not subjected to grinding treatment. This approach aimed to preserve the physical integrity of the solid and mimic real-world conditions. In particular, CEC was assessed following the method 15A1 described by Rayment and Lyons (2011) [38], using 1 M ammonium chloride at pH 7.0 as the extraction solution. The soil-to-solution ratio was maintained at 1:20, and the mixture was shaken for 1 h using an orbital shaker. CEC values were determined by measuring the concentrations of Na^+, K^+, Mg^{2+}, and Ca^{2+} through ICP-OES analysis (Agilent 5800 ICP-OES, Agilent Technologies, Inc., Santa Clara, CA, USA) and reported as meq/100 g of sediment. The pH of the sediment was determined following the standard method [39], while organic matter and carbonate content were quantified through thermogravimetric analysis (TGA). Sediment samples were also analysed to ascertain their mineralogical composition using a Siemens D5000 X-ray diffractometer (Siemens Analytical X-ray Instruments, Inc., Madison, WI, USA), equipped with a Cu Kα radiation source operating at 40 kV and 40 mA, using a 2 mm slit over a 2θ range of 5–60°. Measurements were conducted with a step size of 0.02° and a scanning speed of 1.2° per minute. The

collected data were processed using Xpert HighScore 5.2 software to identify the primary crystalline phases and determine their relative abundances.

Additionally, sediment samples underwent labile extractions to determine the concentrations of weakly bound As and other crustal metals, including Al, Fe and Mn. These geogenic components, commonly found as oxides and hydroxides on sediment and soil surfaces [40], can affect the release and speciation of As [41,42]. 1 M HNO_3 was chosen as the extractant, being the most effective solution for extracting surface-bound elements from sediment [43]. Samples were prepared by accurately weighing 0.03 g of dry sediments into 30 mL LDPE bottles carefully pre-cleaned (as described in Section 2.2). Subsequently, the bottles were filled with ultrapure water and distilled HNO_3 to obtain a final 1 M extracting solution. A series of 6 replicates was performed for each sample. Experiment batches were then placed onto an orbital shaker at 150 rpm for 16 h before being centrifuged at 2500 rpm for 15 min. A 1 mL aliquot was then collected, diluted in 30 mL of ultrapure water and analysed using ICP-MS with Rh as an internal standard (instrument working parameters are described in Table S1 in Supplementary Material).

2.4. Arsenic Adsorption-Desorption Batches

2.4.1. Adsorption Experiments

Batch experiments were undertaken to elucidate the interaction mechanisms governing the absorption process, with a focus on relevant sediment variables, including grain size, mineral composition, and the presence of weakly bound metals originally inherent to the sediment.

For each sediment sample analysed (S1, S2, and S3), two distinct sets of experiments were conducted to monitor the adsorption behaviours of inorganic As species. In the experiments focusing on As(III), LDPE bottles were filled with 5.0 g of dry sediment and 200 mL of a 300 ppb As(III) solution derived from the stock solution. On the other hand, the experiments examining As(V) followed the same procedure using a 300 ppb As(V) solution instead. The sediment-to-solution ratio (25 g/L) was selected for its comparability to a similar study affecting adsorption of metals onto sediment [44]. A set of blanks containing water and sediment, with no added As in solution, were prepared to examine the As desorbed from the sediment under the same adsorption experimental conditions, ensuring that only the As originally present at background levels was monitored. In addition, control blanks without sediment were prepared to assess the stability of As in solution over time. Experiment batches underwent continuous agitation on an orbital shaker set at 150 rpm for a total duration of 196 h. At specific intervals (0.5, 1, 3, 6, 12, 24, 48, 72, 96, 120, 144, 168, 175, and 192 h from the onset of kinetics (t_0)), solution aliquots were withdrawn. Each aliquot of 1.5 mL was then filtered through a 0.45 µm pore syringe filter, transferred to pre-cleaned polyethylene tubes and spiked with 2% HNO_3 for stabilisation before subsequent analysis via ICP-MS using Thermo-Scientific Icap Q ICP-MS instrument (Thermo Fisher Scientific Inc., Waltham, MA, USA). After ICP-MS analysis, the adsorption capacity (Q_T, as mg/kg of adsorbed As by the sediment) of the different sediments for each As oxidation state was calculated using Equation (1) [42,45]:

$$Q_T = Q_b + v/m\ (C_0 - C_t) \quad (1)$$

where Q_b is the background As concentration (mg/kg), v is the volume of the batch solution (L), m is the amount of sediment in the batch (kg), C_0 is the initial As concentration (mg/L), and C_t is the As residual concentration in solution at time t from ICP-MS measurements (mg/L).

The kinetic process of adsorption was analysed using the pseudo-first-order (PFO) and pseudo-second-order (PSO) equations, shown in Equations (2) and (3), respectively:

$$\ln(Qe - Qt) = \ln Qe - k1t \quad (2)$$

$$t/Qt = 1/k_2Qe2 + t/Qe \quad (3)$$

where Qe (μmol/g) and Qt (μmol/g) represent the adsorption capacity values at equilibrium and at a specific time t (min); k1 (1/min) and k2 (g/μmol × min) are the rate constants for the pseudo-first-order and the pseudo-second-order, respectively [46].

Arsenic Adsorption Efficiency (%) at each sampling time (AE_T) was also calculated for each sediment, using Equation (4):

$$AE_T(\%) = (C_0 - C_t)/C_0 \times 100 \quad (4)$$

where AE_T is the efficiency (%), C_0 is the initial As concentration in the batch solution (corrected after the analysis of blank values), and C_t is the residual concentration of As in solution at time t.

The adsorption efficiency results [AE(%)] obtained from the experimental batch tests, together with the sediment properties (D_{50} and Mn-WB) of each sediment used in the adsorption replicates, were employed to generate contour plots illustrating the adsorption efficiency of As(V) and As(III) onto the sediments. For each replicate, only the maximum AE% values, corresponding to the equilibrium condition reached after 144 h, were used to generate the plots. These values, rather than the full kinetic curves, were used to represent the final adsorption efficiencies.

2.4.2. Desorption Experiments

Kinetic desorption experiments were conducted immediately after the completion of the adsorption process to monitor the effective release of the contaminant over time. Initially, the liquid phase was completely removed from the LDPE bottles containing the adsorption experiments. From the same batches employed in adsorption experiments, the sediment was then extracted and rinsed with absolute ethanol (96%) to eliminate the As solution trapped between sediment grains. Subsequently, each sediment sample was oven-dried at 40 °C overnight to evaporate the ethanol [42]. The dry sediments were then weighed to determine any potential material loss due to the recovery process, thus preventing underestimation of metal release into solution. The treated sediment was then introduced into experimental batches in contact with ultrapure water, and the same procedure from the adsorption experiments was applied. A sediment-to-solution ratio of 25 g/L was then maintained, consistent with the conditions of the previous adsorption experiments. Similar to the adsorption experiments, the solutions were subjected to continuous agitation for 192 h, and aliquots were extracted for subsequent analysis using ICP-MS. Desorption data were obtained through Equation (5) [45]:

$$Q_{DES} = C_D \times v/m \quad (5)$$

where Q_{DES} represents the amount of As desorbed from the sediment (mg/kg), C_D is the concentration of As at time t after the desorption experiment (mg/L), v is the volume of the solution (L) and m is the sediment weight (kg).

Arsenic Desorption Efficiency (%) at equilibrium time (DE_{EQ}) was also calculated for each sediment, using Equation (6):

$$DE_{EQ}(\%) = [Q_{T(EQ)} - Q_{DES(EQ)}]/Q_{T(EQ)} \times 100 \quad (6)$$

where DE_{EQ} is the efficiency (%), $Q_{T(EQ)}$ is the sediment adsorption capacity from adsorption experiments at equilibrium time (144 h), and $Q_{DES(EQ)}$ is the As concentration$_{(sed)}$ after desorption at the equilibrium time (144 h).

2.5. Statistical Analyses

Prior to applying any statistical tool to the As adsorption and desorption results, a one-way analysis of variance (ANOVA) was conducted to determine whether significant differences existed among the three selected sediment samples (S1, S2, and S3) based on their measured physicochemical properties. The objective was to assess whether inter-group variability was statistically significant for key sediment variables, thereby justifying their inclusion as predictors in subsequent modelling of As behaviour. Each single-factor ANOVA involved three groups (corresponding to S1, S2, and S3), with six replicate measurements per group for each tested parameter.

Following ANOVA, simple linear regression (SLR) was applied to investigate the relationships between individual sediment properties and As adsorption/desorption capacity. The input dataset comprised 18 observations (6 replicates for each of the 3 sediment types), arranged as an 11 × 18 matrix. Of these, 7 columns represented sediment properties, which were treated as explanatory variables (weakly bound elements: As-, Al-, Mn-, Fe-WB; grain size: $D_{50;}$ sediment pH; CEC). The remaining 4 columns represented adsorption and desorption efficiencies for As(V) and As(III), which were treated as response variables (experimental maximum adsorption, Q_T, and desorption, Q_{DES}, corresponding to the final plateau concentrations at 144 h, rather than full kinetic time-series data). For each regression model, a single explanatory variable was tested against one response variable. Each observation was treated as statistically independent, reflecting the variability observed within and across sediment groups.

Mineralogical information obtained from XRD (calcite, quartz, feldspars, and phyllosilicates content) was not included as quantitative predictors in the regression models; instead, these semi-quantitative data were used qualitatively to support interpretation of As sorption behaviours.

Prior to regression analysis, data normalisation was performed using z-score normalisation [47], represented by Equation (7):

$$z = (x - m)/\sigma \quad (7)$$

where m is the average value of the variable data population, σ is the population standard deviation and x is the single value taken into consideration for the z-normalisation. Normalisation was adopted to facilitate the identification of variations in variables across different samples and compare different geochemical properties originally represented by different scales and units.

3. Results and Discussion

3.1. Sediment Characteristics

3.1.1. GSD–Grain Size Distribution

The overall grain size distribution showed high variability in the samples analysed. Sample composition exhibited disparities, both in terms of grain size uniformity and sediment heterogeneity. As expected, results showed a correlation between the depth of the sediment core extraction and the size distribution profile, with a discernible trend towards finer grains at greater depths (Figure 3). Overall, the results align with previous studies on the composition and stratigraphy of Como subsoil [5]. In particular, sample S1 emerged as the most heterogeneous and coarsest among the three (Table S2 in Supplementary Material).

Samples S2 and S3, instead, exhibited a distinct grain size distribution, predominantly comprising silty particles. This clear difference between the former sample and the latter two suggests a transitional sedimentary environment, from a silty palustrine deposition to more stable, low-energy conditions, typically associated with glaciolacustrine sediments [22].

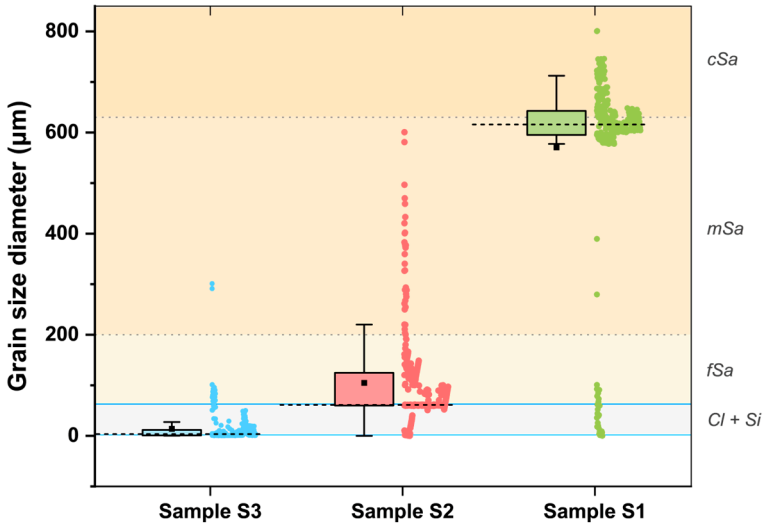

Figure 3. Box plot of Grain Size Diameter data for each sample. Coloured dots represent measurements, dashed lines over boxes represent median value, while the mean value is represented by a full square. Dotted lines are the limits to the classification of fine sand (fSa), medium sand (mSa), and coarse sand (cSa). Light blue lines represent the upper and lower limits of the classification of clay and silt. Values used for the limits definition are reported in Table S2 in Supplementary Material.

3.1.2. Geochemistry and Mineralogy

The geochemical and mineralogical analysis of the sediment samples provided important insights into the factors influencing the adsorption and desorption of As species. Results for pH, cation exchange capacity (CEC), weakly bound metal concentrations, and organic matter content highlighted significant trends related to sediment depth. Results show vertical changes between the samples analysed. As depth increased, a general decrease in pH and CEC values (Table 1) was observed, both of which are critical in influencing As retention due to their impact on the ability of sediments to retain charged metal ions. The concentrations of weakly bound elements such as As (As-WB), Al (Al-WB), Mn (Mn-WB), and Fe (Fe-WB) were measured in water extracts (Table 1). The highest As-WB concentration was recorded in sample S1, which correlates with the highest CEC and pH, suggesting an increased potential for As retention. Al-WB and Mn-WB concentrations also showed a declining trend with depth, while Fe-WB concentrations were slightly lower in sample S3 compared to S1 and S2. The presence of these metals, particularly Fe, is significant, as Fe-oxides and hydroxides are known to be effective adsorbents for As [48]. Organic matter content showed low similar values across all samples (Table 1). Mineralogical analyses, based on X-ray diffraction (XRD) spectra (Figure S1, Supplementary Material), indicate the presence of calcite, quartz, feldspars (including albite, amphibole, and orthoclase), and phyllosilicates (mainly represented in the samples as muscovite, antigorite and chlorite) (Table 1). Calcite was found to be most abundant at shallow depths, with a notable decrease in deep sediments (both S2 and S3). This distribution aligns with the higher pH and CEC values of the shallowest sediments, suggesting the effect of calcite in maintaining alkaline conditions. Quartz and feldspars were consistently present across different depths, with similar relative abundances. Only sample S1 exhibited a lower presence of feldspars,

lacking in amphibole and orthoclase. Phyllosilicates instead showed the highest relative abundance at shallow depth and decreased in amount with increasing depth, reflecting the compositional variability of the sampled glaciolacustrine deposit [22].

Table 1. Geochemical and mineralogical properties of sediment at different depths (S1: 50 m, S2: 60 m, and S3: 70 m). The table presents measurements of sediment pH, CEC, weakly bounded metals (As, Al, Mn, and Fe), organic matter content (OM) and main mineralogical phases (relative mineral abundances are indicated with "+", more plus signs denote higher abundance, refer to Figure S1 in Supplementary Material for XRD spectra).

	Sample S1	Sample S2	Sample S3
Sediment pH	7.86 ± 0.13	6.54 ± 0.16	6.89 ± 0.09
CEC (meq/100 g)	39.62 ± 1.067	26.27 ± 1.561	24.03 ± 0.901
As-WB (ppb)	8.491 ± 0.503	5.631 ± 0.457	4.825 ± 0.325
Al-WB (ppm)	8.616 ± 0.285	6.896 ± 0.095	5.675 ± 0.073
Mn-WB (ppb)	385.813 ± 3.499	256.854 ± 2.557	248.893 ± 1.222
Fe-WB (ppm)	15.815 ± 0.149	14.503 ± 0.592	11.888 ± 0.191
OM (%)	0.31	0.37	0.36
Calcite	+++	++	+
Quartz	+	++	++
Feldspars	+	++	++
Phyllosilicates	+++	++	+

3.2. As(V) and As(III) Adsorption and Desorption: Experimental Results

The kinetic adsorption experiments for As(V) and As(III) (Figure 4a,b) revealed a rapid initial uptake within the first 12 h for all sediment samples tested, followed by a pronounced decrease in adsorption rate after 24 h, approaching equilibrium for the remaining duration of the experimental period. For As(V), maximum adsorption efficiency was attained after 72 h, with nearly complete removal of the initial dissolved concentration after 144 h. Sediment S1 exhibited the highest removal efficiency (>80%), whereas sediments S2 and S3 reached lower efficiencies (around 60%) (Figure 5a). In contrast, As(III) adsorption was less efficient overall, with minimal variation between sediment types (Figures 4b and 5b). These initial findings suggest a higher affinity of the sediments, particularly S1, for As in its pentavalent form. This preferential adsorption of As(V), generally present in water as an oxyanion (e.g., $H_2AsO_4^-$ or $HAsO_4^{2-}$) tends to form inner-sphere complexes with mineral surfaces, particularly Fe- and Al-oxides [49]. As(III), on the other hand, typically exists as the neutral species H_3AsO_3 under circumneutral pH and interacts more weakly with mineral surfaces, resulting in reduced adsorption and greater mobility [15]. The limited variation among sediments in As(III) adsorption further reflects its weak and largely non-specific interaction under the tested conditions.

Adsorption kinetics for both species were globally well described by fitting to the pseudo-second-order model (average $R^2 > 0.99$; Table S3 in Supplementary Material), consistent with chemisorption being the rate-limiting step and in agreement with previous reports on trace metal-sediment interactions [15,50]. This is consistent with literature findings that chemisorption, involving specific surface complexation, governs the long-term retention of both As species in natural sediments [51]. Conversely, the pseudo-first-order model provided a better fit during the initial adsorption phase (Figure S2, Supplementary Material), suggesting that early uptake may occur at lower-energy surface sites (e.g., possibly associated with Fe- and Al- oxides) via rapid, outer-sphere complexation [52]. As these sites become progressively occupied, the process transitions to high-energy chemisorption, which is more accurately captured by the pseudo-second-order model. This potential

two-step behaviour implies that both surface diffusion and chemical bonding may play a role in overall As retention on sediments.

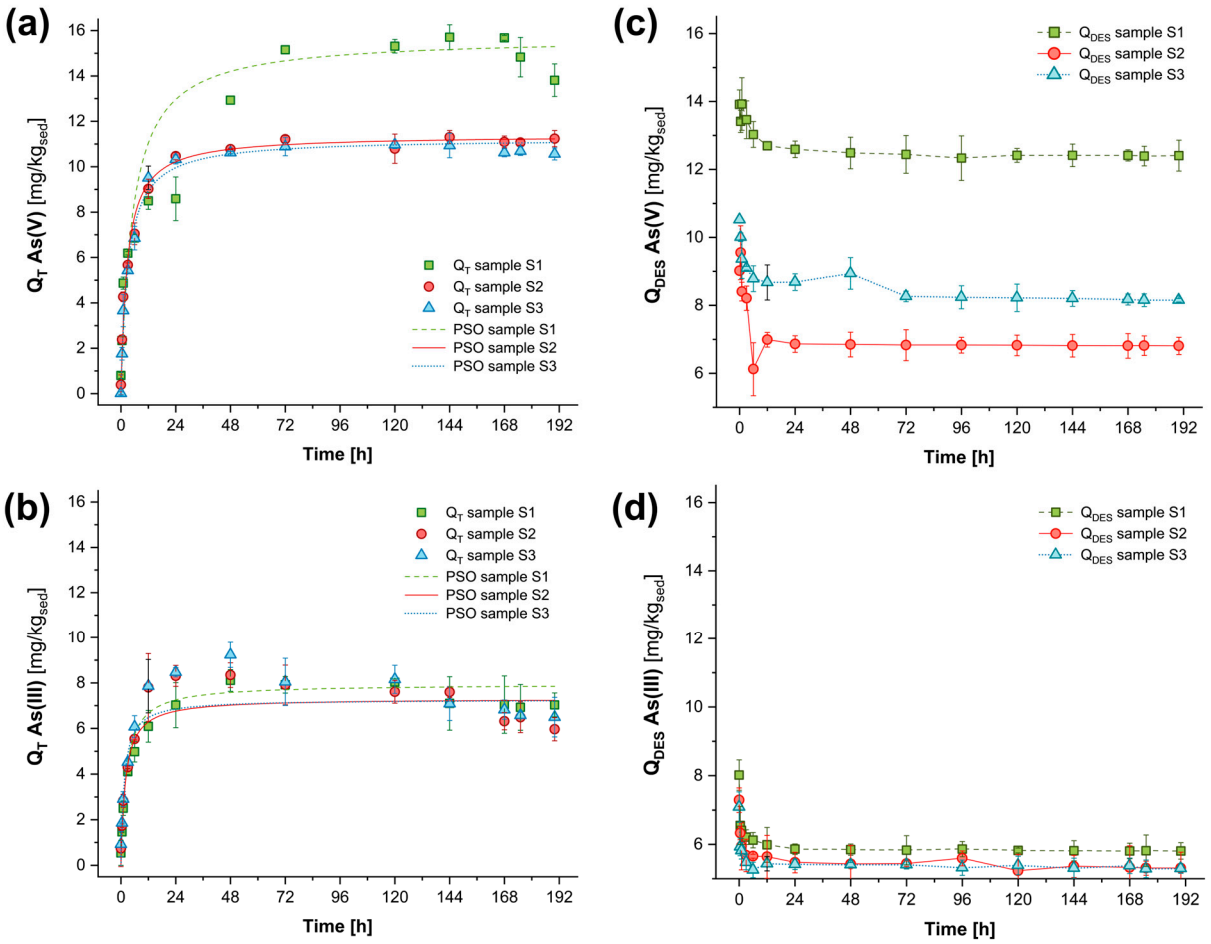

Figure 4. Adsorption kinetics onto tested sediments for (**a**) As(V) and (**b**) As(III), starting from 300 ppb solutions in ultrapure water (6 replicates for each data point). Pseudo-second-order (PSO) fittings are shown as solid and dashed lines, respectively. Desorption kinetics are presented in panel (**c**) As(V) and panel (**d**) As(III).

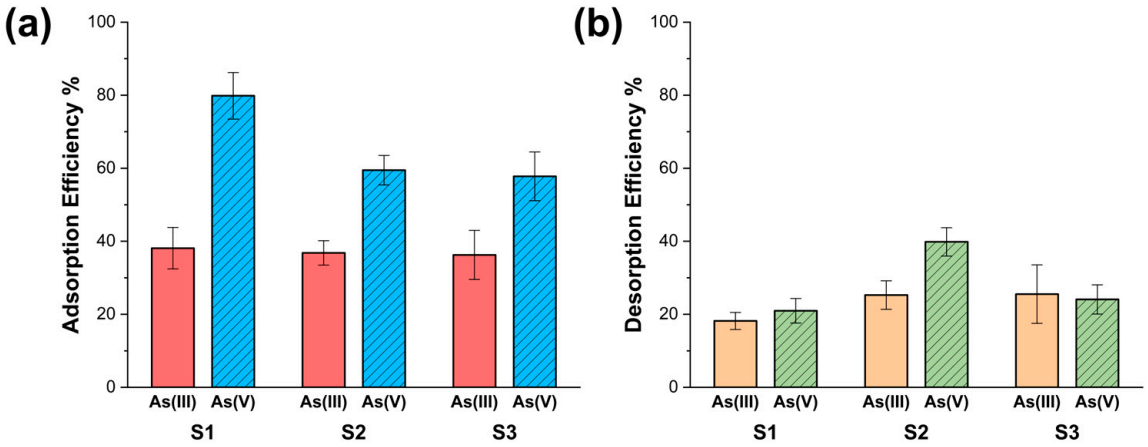

Figure 5. Adsorption (**a**) and desorption (**b**) efficiencies (%) of As(III) and As(V) on experimental sediments. Plotted values represent the mean of six experimental replicates, measured at the maximum adsorption and desorption points at 144 h.

On the other hand, desorption kinetic experiments (Figure 4c,d) showed that the amount of As released was substantially lower than the quantity adsorbed, indicating that a portion of the metalloid adsorbed irreversibly under the applied experimental conditions. On average, only ~30% of previously adsorbed As was released (Figure 5b), leading to ~70% of As retained by sediment. Furthermore, for As(V), desorption from S1 was notably lower than from S2, likely reflecting the higher initial adsorption and stronger inorganic bonds on S1 surfaces [36,41]. This observation supports the idea that oxide-rich sediments, such as S1, may provide a more reactive surface area for inner-sphere complex formation and permanent sequestration of arsenate [37]. In contrast, As(III) desorption showed no significant differences among sediment types, consistent with the negligible variation observed during its adsorption phase. This reinforces the interpretation that As(III) interactions with the sediment matrix were relatively weak and reversible under the tested conditions, leading to higher potential mobility in natural systems.

Finally, it should be acknowledged that the batch experiments were conducted under oxic laboratory conditions in sealed containers, without specific control of redox potential, and As speciation was not measured after the reaction. While As(V) and As(III) were introduced independently, partial oxidation of As(III) to As(V) cannot be excluded, particularly over longer timeframes. However, the consistently lower adsorption efficiency and the lack of correlation with sediment properties observed for As(III) suggest that any interconversion was likely limited or did not significantly affect the experimental outcomes.

3.3. As(V) and As(III) Adsorption and Desorption: Statistical Results

3.3.1. Sediment Characteristics ANOVA Results

The ANOVA results indicated that several physicochemical variables, including weakly bound element concentrations, pH, cation exchange capacity (CEC), and grain size (D_{50}), exhibited statistically significant differences among sediment groups, as evidenced by *p*-values < 0.01 and F-statistics exceeding critical thresholds (Table 2). This outcome supports the existence of meaningful between group variance for these properties, supporting their potential role as discriminant factors among sediment types. In contrast, organic matter content (OM%) did not display significant variability across groups; the null hypothesis could not be rejected, suggesting that OM% likely exerts a limited influence on the differences in As behaviour observed in this study. Accordingly, OM% was excluded from subsequent statistical analyses and will not be discussed further in the interpretation of adsorption-desorption results.

Table 2. One-way analysis of variance (ANOVA) test results for sediment properties between sample groups S1, S2, and S3.

Source of Variation	d.f.	SS	MS	F-Value	*p*-Value
D_{50}	2	1,371,809.027	685,904.514	1849.031	**0.0000**
pH	2	5.612	2.806	138.626	**0.0000**
CEC	2	733.893	366.946	144.781	**0.0000**
As-WB	2	44.538	22.269	98.103	**0.0000**
Al-WB	2	26.197	13.099	342.615	**0.0000**
Mn-WB	2	70,881.775	35,440.888	4370.124	**0.0000**
Fe-WB	2	47.962	23.981	146.530	**0.0000**
OM%	2	0.006	0.003	2.371	0.1356

Note: d.f, degrees of freedom; SS, sum of squares; MS, mean square; (F-crit = 3.68). Bold *p*-values indicate high statistical significance (<0.001).

Mineralogical variables (calcite, quartz, feldspars, and phyllosilicates relative abundances) were not subjected to ANOVA testing because their within-group variance was zero. The lack of variability arose from the fact that these data were derived from identical XRD spectra obtained for each replicate within a sediment group, yielding identical semi-quantitative mineralogical composition for S1, S2, and S3 subsamples. As a result, statistical comparison across XRD output replicates was mathematically redundant, and performing ANOVA under such conditions would have been inappropriate and uninformative. Although this prevented statistical comparison within groups, the differences in average mineralogical composition between groups were sufficiently distinct to support meaningful interpretation in relation to As adsorption-desorption behaviour. Therefore, mineralogical data are presented descriptively, with emphasis on their role in explaining observed trends.

3.3.2. Sediment Predictors of As Adsorption and Desorption

To assess the influence of individual sediment properties on As mobility, simple linear regressions were performed between each measured independent variable and the experimentally determined maximum adsorption (Q_T) and desorption (Q_{DES}) values for As(V) and As(III). A threshold of $R^2 \geq 0.90$ was applied to highlight the most predictive relationships, with interpretation focused on statistically robust correlations.

For As(V) adsorption, several variables showed strong and significant relationships ($p < 0.001$) with Q_T, including Mn-WB ($R^2 = 0.943$), As-WB ($R^2 = 0.936$), Al-WB ($R^2 = 0.904$), and grain size (D_{50}, $R^2 = 0.941$) (SLR results are reported in Table 3). The association with Mn- and Al-(hydr)oxides is consistent with their dual role as potent oxidants and sorbents, facilitating As(V) chemisorption through surface complexation, as widely documented in recent literature [40]. These phases, often occurring as coatings on mineral grains, likely enhance retention capacity. Although the prevailing view is that fine particles (<425 µm) provide the most reactive surface area [53,54], in this study larger sizes were associated with higher adsorption efficiencies. This positive effect of coarser textures could be explained by their correlation with elevated Mn-WB contents. The contour plot in Figure 6 illustrates a clear positive linear relationship between D_{50} and Mn-WB, with sediment adsorption efficiencies approaching 85% at high Mn-WB levels and coarser textures, consistent with findings from Schacht & Ginder-Vogel [55]. The presence of Mn-(hydro)oxides on sediment surfaces also played an important role in the desorption of As(V), possibly highlighting the dual role of these functional groups in both adsorption and release processes. This behaviour is coherent with previous studies showing that As(V) binding to Mn-(hydro)oxides is generally weaker and more reversible compared to the stronger chemisorption observed on Fe-oxides [56]. By contrast, in the present study, Fe-oxides appear to have contributed less to the overall adsorption/desorption dynamics, as also suggested by the SLR results, likely due to their relatively low abundance in the sediments compared to Mn phases.

Moreover, for As(V) desorption, Q_{DES} was most strongly correlated with pH ($R^2 = 0.938$), CEC ($R^2 = 0.938$) and D_{50} ($R^2 = 0.900$), indicating that both sediment chemical conditions and grain influence the reversibility of arsenate binding. In addition, qualitative inspection of the XRD results suggests that mineralogical composition further modulates these processes: sediments richer in phyllosilicates tended to retain arsenate more strongly, whereas quartz-rich samples exhibited greater desorption potential.

Table 3. Results of simple linear regression (SLR) analysis between sediment properties (explanatory variables) and As adsorption/desorption capacities (response variables) for As(V) and As(III). Regression was performed after z-score normalisation; therefore, coefficients are normalised and directly comparable across variables. For each model, the regression coefficient, *p*-value, and coefficient of determination (R^2) are reported. Values corresponding to models with $R^2 \geq 0.90$ are highlighted in bold.

		ADSORPTION			DESORPTION		
	Explanatory Variable	***Coefficient***	***p-Value***	***R^2***	***Coefficient***	***p-Value***	***R^2***
As(V)	**As-WB**	**0.967**	**0.000**	**0.936**	0.864	0.000	0.747
	Al-WB	**0.951**	**0.000**	**0.904**	0.779	0.000	0.607
	Mn-WB	**0.971**	**0.000**	**0.943**	**0.956**	**0.000**	**0.915**
	Fe-WB	0.839	0.000	0.704	0.569	0.014	0.324
	D_{50}	**0.970**	**0.000**	**0.941**	**0.943**	**0.000**	**0.900**
	$pH_{(SED)}$	0.843	0.000	0.711	**0.969**	**0.000**	**0.938**
	CEC	0.743	0.000	0.589	**0.949**	**0.000**	**0.901**
As(III)	**As-WB**	0.359	0.143	0.129	0.643	0.004	0.414
	Al-WB	0.327	0.185	0.107	0.635	0.005	0.404
	Mn-WB	0.223	0.374	0.050	0.667	0.002	0.445
	Fe-WB	0.362	0.139	0.131	0.652	0.003	0.426
	D_{50}	0.218	0.385	0.048	0.648	0.004	0.420
	$pH_{(SED)}$	0.048	0.849	0.002	0.526	0.025	0.277
	CEC	0.203	0.419	0.041	0.690	0.002	0.476

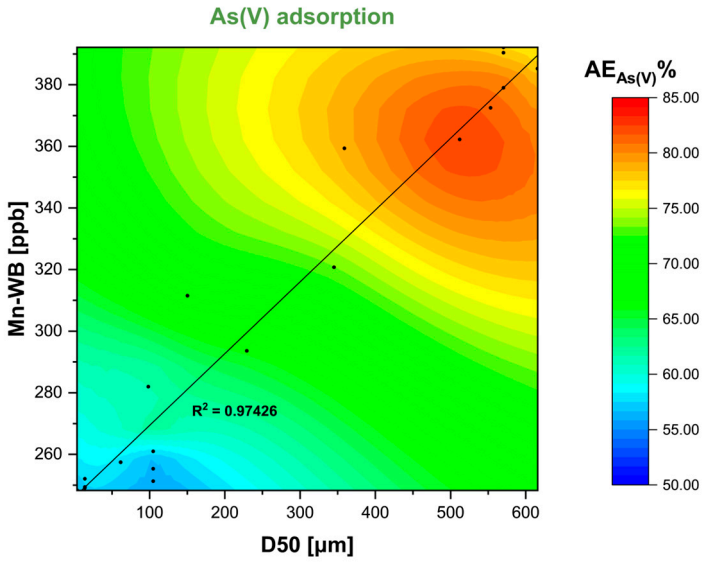

Figure 6. Contour plot showing As(V) adsorption efficiency (AE%) as a function of D_{50} and Mn-WB content, with warmer colours indicating higher adsorption efficiency. Black dots represent measured data (n = 18), and the fitted regression yields R^2 = 0.97.

By contrast, As(III) adsorption exhibited low predictive power across all variables ($R^2 < 0.15$, with non-significant *p*-values), suggesting that within the scope of this study's design, no single measured sediment property adequately explains its retention. This is consistent with kinetic experiments showing generally lower As(III) uptake compared to As(V), attributable to its weaker affinity for oxide minerals and differing surface complexation mechanisms. Furthermore, for As(III) desorption, moderate relationships were observed with CEC (R^2 = 0.476, *p*-value < 0.01), Mn-WB (R^2 = 0.445, *p*-value < 0.01), and Fe-WB (R^2 = 0.426, *p*-value < 0.01), although these were considerably weaker than those for As(V). This again aligns with experimental observations that As(III) release is less predictable

and likely influenced by multiple interacting factors, including redox transformations not captured by static sediment metrics.

3.4. Implication for As Mobility in the Como Aquifer

The findings from this study provide insights into the possible mechanisms driving inorganic As mobility within the Como aquifer system, allowing comparison between experimentally derived adsorption-desorption results and observed groundwater concentrations [5].

The predominance of Mn- and Al-(hydr)oxides-rich, coarser-grained shallow sediments corresponds to lower dissolved As levels. This characteristic of the sediment (e.g., S1) furthermore enhances minimal desorption, indicating stable As retention likely mediated by chemisorption and complexation mechanisms [56]. Such retention capacity is consistent with the relatively lower dissolved As concentrations measured in Como shallow groundwater, where these sediment types predominate.

In contrast, deeper horizons (e.g., S2 and S3) demonstrated lower adsorption capacities in laboratory tests, in agreement with the elevated dissolved As concentrations observed in groundwater at comparable depths. The reduced retention potential of these deeper sediments suggests that once mobilised, particularly in the more weakly adsorbed As(III) form, As is less likely to be removed from solutions.

In the sediments analysed, organic matter content was generally low. Previous studies have shown a higher affinity of As(III) for OM-rich fractions [57], suggesting that the low OM levels in our samples may have contributed to the reduced As(III) retention observed. However, the narrow OM range limits the ability to draw broader conclusions on its predictive role.

From an aquifer-scale perspective, the results obtained here reinforce the importance of redox processes in controlling As mobility in the Como system. Although the present data did not show evidence of significant organic matter–mediated transformations, the observed dominance of As(III) in desorption products indicates that redox-driven conversion from As(V) to As(III) could substantially increase mobility in sediment zones with lower adsorption capacity. Such conditions may occur in parts of the aquifer where As(V) derived from potential sources such as thermal fluids (e.g., [58]) interacts with mineral assemblages less effective in retaining As. These implications suggest that areas with reduced adsorption potential could be more sensitive to geochemical fluctuations (e.g., pH and redox shifts), thereby warranting closer hydrogeochemical monitoring to assess the risk of As release under changing environmental conditions.

4. Conclusions

The adsorption-desorption behaviour of As(V) and As(III) was investigated through controlled batch experiments on three sediments collected from distinct depths of the Como aquifer. The selected samples were intended to represent contrasting physicochemical properties and to reflect the vertical variability in aquifer composition and groundwater As concentrations. Experimental outcomes, interpreted alongside ANOVA and regression analyses, showed that the maximum adsorption capacity of sediments varies markedly between As species. As(V) exhibited consistently higher adsorption efficiency and lower desorption than As(III), with its retention strongly correlated ($R^2 > 0.90$) with Mn- and Al-(hydr)oxide content, grain size, and mineralogical composition (mainly quartz and feldspar content). These results are further supported by the excellent fit of adsorption data to the pseudo-second-order (PSO) kinetic model ($R^2 > 0.99$), consistent with chemisorption as the dominant retention mechanism for As(V). In contrast, As(III) adsorption displayed

no strong dependence on individual sediment properties, reflecting its lower affinity for mineral surfaces.

Comparison of these experimental results with groundwater data previously reported in literature shows that shallow aquifer zones, where dissolved As levels are typically below 10 μg/L, coincide with coarse-grained, Mn- and Al-rich sediments that here demonstrated high As(V) retention and minimal desorption. Conversely, deeper aquifer layers, where concentrations can reach ~250 μg/L, correspond to finer-grained sediments with lower oxide content and reduced adsorption capacity, which in our experiments released proportionally more As(III) during desorption. This alignment between laboratory behaviour and field measurements supports the role of sediment mineralogy and texture as key controls on the vertical distribution of As in the Como aquifer.

While mineralogical differences were clearly reflected in As(V) behaviour, the response of As(III) remained poorly correlated with the sediment properties evaluated. The role of other sediment components, such as organic matter, remains less conclusive. Previous studies have highlighted the strong influence of organic matter (OM) on As(III) adsorption, due to its ability to modify redox conditions, form aqueous complexes, or compete for surface sites. However, in the present study, the relatively uniform OM content across all sediment samples may have limited the ability to capture this effect. This could partly explain why none of the tested sediment properties emerged as significant predictors for As(III) retention, despite its adsorption kinetics being well described by a pseudo-second-order model, typically associated with chemisorption. It is therefore plausible that OM-related interactions, not fully accounted for in this dataset, represent a key factor underlying the modelled chemisorption behaviour of As(III). Broader environmental and compositional ranges, combined with in situ redox monitoring and advanced speciation analyses, would allow a more comprehensive understanding of the coupled roles of organic matter, mineral phases, and redox transformations.

It is also acknowledged that redox conditions were not tightly controlled during the batch experiments, and As speciation was not monitored post-reaction. While As(V) and As(III) were introduced independently, partial oxidation of As(III) to As(V) may have occurred over time, given the toxic laboratory conditions. However, the consistently lower adsorption efficiency observed for As(III) suggests that any interconversion was limited or did not substantially influence the outcome. Still, this represents an experimental limitation and highlights the need for future studies to incorporate post-experimental speciation analysis to better constrain redox-related transformations. Despite this, the results remain valuable for understanding As mobility under realistic environmental conditions, where similar redox processes are likely to occur naturally.

Overall, the results provide a mechanistic basis for explaining the vertical variability of As in the Como aquifer and offer a framework for improving groundwater monitoring and management strategies in multilayer aquifer systems.

Supplementary Materials: The following supporting information can be downloaded at: https://www.mdpi.com/article/10.3390/w17172616/s1. Supporting information is presented in Supplementary Material. Figure S1: XRD spectra of sediment samples. Relevant peak patterns of the main minerals present in the samples are indicated by the abbreviations (Qz: quartz, Mu: muscovite, Ant: antigorite, Ca: calcite, Amp: amphibole, Chl: chlorite, Alb: albite, Ort: orthoclase); Figure S2: PFO and PSO model curves for As(V) and As(III) adsorptions; Table S1: ICP-MS working parameters. LODs were calculated as three times the standard deviations of blank samples; Table S2: Samples particle size distribution (classification based on EN ISO 14688-1:2017); Table S3: PFO and PSO models; Figure S3: As(V) (a) and As(III) (b) adsorption efficiency (AE%) in relation to Mn-WB concentrations and particle grain size (D_{50}).

Author Contributions: Conceptualisation, S.T. and G.B.; methodology, S.T. and G.B.; software, S.T. and G.B.; validation, S.T. and G.B.; formal analysis, S.T.; investigation, S.T. and G.B.; resources, G.B., A.P. and A.M.M.; data curation, S.T. and G.B.; writing—original draft preparation, S.T.; writing—review and editing, all authors; visualisation, S.T. and G.B.; supervision, G.B., A.P. and A.M.M.; project administration, A.M.M.; funding acquisition, A.M.M. All authors have read and agreed to the published version of the manuscript.

Funding: The authors are thankful to the European Union—NextGenerationEU—Mission 4 "Education and Research"—Component 2 "From Research to Business"—Investment 3.1 "Fund for the realization of an integrated system of research and innovation infrastructures"—Project IR0000037—GeoSciences IR-CUP I53C22000800006, for providing a scholarship to the first author to undertake this study.

Data Availability Statement: The original contributions presented in this study are included in the Supplementary Materials. Further enquiries can be directed to the corresponding author.

Acknowledgments: The authors wish to thank Francesca Ferrario for her assistance in sampling processes. Scientific support from the CRIETT centre of the University of Insubria (instrument code: MAC10) is greatly acknowledged.

Conflicts of Interest: The authors declare no conflicts of interest.

Abbreviations

The following abbreviations are used in this manuscript:

As(V)	Arsenate
As(III)	Arsenite
CEC	Cation Exchange Capacity
GSD	Grain Size Distribution
ICP-MS	Inductively Coupled Plasma Mass Spectrometry
ICP-OES	Inductively Coupled Plasma Optical Emission Spectroscopy
SLR	Simple Linear Regression
ANOVA	Analysis of Variance
PFO	Pseudo-First-Order (Kinetic model)
PSO	Pseudo-Second-Order (Kinetic model)
QA/QC	Quality Assurance/Quality Control
XRD	X-ray Diffraction
LDPE	Low-Density Polyethylene
TGA	Thermogravimetric Analysis
OM	Organic Matter
WB	Weakly Bound (referred to elements)

References

1. Bhat, A.; Ravi, K.; Tian, F.; Singh, B. Arsenic Contamination Needs Serious Attention: An Opinion and Global Scenario. *Pollutants* **2024**, *4*, 196–211. [CrossRef]
2. Sevak, P.; Pushkar, B. Arsenic Pollution Cycle, Toxicity and Sustainable Remediation Technologies: A Comprehensive Review and Bibliometric Analysis. *J. Environ. Manag.* **2024**, *349*, 119504. [CrossRef]
3. Nordstrom, D.K. Worldwide Occurrences of Arsenic in Ground Water. *Science* **2002**, *296*, 2143–2145. [CrossRef]
4. Podgorski, J.; Berg, M. Global Threat of Arsenic in Groundwater. *Science* **2020**, *368*, 845–850. [CrossRef] [PubMed]
5. Binda, G.; Frascoli, F.; Spanu, D.; Ferrario, M.F.; Terrana, S.; Gambillara, R.; Trotta, S.; Noble, P.J.; Livio, F.A.; Pozzi, A.; et al. Geochemical Markers as a Tool for the Characterization of a Multi-Layer Urban Aquifer: The Case Study of Como (Northern Italy). *Water* **2022**, *14*, 124. [CrossRef]
6. Wang, N.; Ye, Z.; Huang, L.; Zhang, C.; Guo, Y.; Zhang, W. Arsenic Occurrence and Cycling in the Aquatic Environment: A Comparison between Freshwater and Seawater. *Water* **2023**, *15*, 147. [CrossRef]

7. Raju, N.J. Arsenic in the Geo-Environment: A Review of Sources, Geochemical Processes, Toxicity and Removal Technologies. *Environ. Res.* **2022**, *203*, 111782. [CrossRef]
8. Mollehuara Canales, R.; Guan, H.; Bestland, E.; Hutson, J.; Simmons, C.T. Particle-Size Effects on Dissolved Arsenic Adsorption to an Australian Laterite. *Environ. Earth Sci.* **2013**, *68*, 2301–2312. [CrossRef]
9. Yang, H.-J.; Lou, C.-Y. *Arsenic in Chianan Plain Sediments from SW Taiwan: Causes of Concentration and Potential of Release to Groundwater*; CRC Press: Boca Raton, FL, USA, 2024; pp. 129–130, ISBN 978-1-003-31739-5.
10. Carneiro, M.A.; Pintor, A.M.A.; Boaventura, R.A.R.; Botelho, C.M.S. Current Trends of Arsenic Adsorption in Continuous Mode: Literature Review and Future Perspectives. *Sustainability* **2021**, *13*, 1186. [CrossRef]
11. Rehman, A.; Rukh, S.; Ayoubi, S.A.; Khattak, S.A.; Mehmood, A.; Ali, L.; Khan, A.; Malik, K.M.; Qayyum, A.; Salam, H. Natural Clay Minerals as Potential Arsenic Sorbents from Contaminated Groundwater: Equilibrium and Kinetic Studies. *Int. J. Environ. Res. Public Health* **2022**, *19*, 16292. [CrossRef]
12. Verbeeck, M.; Thiry, Y.; Smolders, E. Soil Organic Matter Affects Arsenic and Antimony Sorption in Anaerobic Soils. *Environ. Pollut.* **2020**, *257*, 113566. [CrossRef] [PubMed]
13. Wang, S.; Mulligan, C.N. Effect of Natural Organic Matter on Arsenic Release from Soilsand Sediments into Groundwater. *Environ. Geochem. Health* **2006**, *28*, 197–214. [CrossRef]
14. Welch, A.H.; Westjohn, D.B.; Helsel, D.R.; Wanty, R.B. Arsenic in Ground Water of the United States: Occurrence and Geochemistry. *Groundwater* **2000**, *38*, 589–604. [CrossRef]
15. Nguyen, K.T.; Navidpour, A.H.; Ahmed, M.B.; Mojiri, A.; Huang, Y.; Zhou, J.L. Adsorption and Desorption Behavior of Arsenite and Arsenate at River Sediment-Water Interface. *J. Environ. Manag.* **2022**, *317*, 115497. [CrossRef]
16. Saha, S.; Reza, A.H.M.S.; Roy, M.K. Arsenic Geochemistry of the Sediments of the Shallow Aquifer and Its Correlation with the Groundwater, Rangpur, Bangladesh. *Appl. Water Sci.* **2021**, *11*, 166. [CrossRef]
17. Wang, S.; Chang, Y.; Huang, W.; Yang, D.; Che, F. Release Characteristics of Arsenic from Sediments and Its Source or Sink Competition with Phosphorus: A Case of a Great Lake with Grass-Algae Alternation. *J. Environ. Sci.* **2025**, *149*, 278–287. [CrossRef]
18. Bosi, E.; Colombera, L.; Mountney, N.P.; Bertoni, D.; Sarti, G.; Amorosi, A. Sedimentary Controls on Arsenic Distribution in Meander-Belt Deposits of the Po Valley, Italy. *Sci. Total Environ.* **2025**, *965*, 178627. [CrossRef] [PubMed]
19. Hafeznezami, S.; Zimmer-Faust, A.G.; Dunne, A.; Tran, T.; Yang, C.; Lam, J.R.; Reynolds, M.D.; Davis, J.A.; Jay, J.A. Adsorption and Desorption of Arsenate on Sandy Sediments from Contaminated and Uncontaminated Saturated Zones: Kinetic and Equilibrium Modeling. *Environ. Pollut.* **2016**, *215*, 290–301. [CrossRef]
20. Singh, P.; Sarswat, A.; Pittman, C.U.; Mlsna, T.; Mohan, D. Sustainable Low-Concentration Arsenite [As(III)] Removal in Single and Multicomponent Systems Using Hybrid Iron Oxide–Biochar Nanocomposite Adsorbents—A Mechanistic Study. *ACS Omega* **2020**, *5*, 2575–2593. [CrossRef]
21. Kim, L.; Thanh, N.T.; Toan, P.V.; Minh, H.V.T.; Kumar, P. Removal of Arsenic in Groundwater Using Fe(III) Oxyhydroxide Coated Sand: A Case Study in Mekong Delta, Vietnam. *Hydrology* **2022**, *9*, 15. [CrossRef]
22. Ferrario, M.F.; Bonadeo, L.; Brunamonte, F.; Livio, F.; Martinelli, E.; Michetti, A.M.; Censi Neri, P.; Chiessi, V.; Comerci, V.; Höbig, N. Late Quaternary Environmental Evolution of the Como Urban Area (Northern Italy): A Multidisciplinary Tool for Risk Management and Urban Planning. *Eng. Geol.* **2015**, *193*, 384–401. [CrossRef]
23. Monticelli, D.; Pozzi, A.; Ciceri, E.; Giussani, B. Interpreting Complex Trace Element Profiles in Sediment Cores from a Multi-Basin Deep Lake: The Western Branch of Lake Como. *Int. J. Environ. Anal. Chem.* **2011**, *91*, 213–229. [CrossRef]
24. Comerci, V.; Capelletti, S.; Michetti, A.M.; Rossi, S.; Serva, L.; Vittori, E. Land Subsidence and Late Glacial Environmental Evolution of the Como Urban Area (Northern Italy). *Quat. Int.* **2007**, *173–174*, 67–86. [CrossRef]
25. World Health Organization. *Guidelines for Drinking-Water Quality: Fourth Edition Incorporating First Addendum*, 4th ed. + 1st add.; World Health Organization: Geneva, Switzerland, 2017; ISBN 978-92-4-154995-0.
26. Monticelli, D.; Castelletti, A.; Civati, D.; Recchia, S.; Dossi, C. How to Efficiently Produce Ultrapure Acids. *Int. J. Anal. Chem.* **2019**, *2019*, e5180610. [CrossRef]
27. Binda, G.; Pozzi, A.; Livio, F.; Piasini, P.; Zhang, C. Anomalously High Concentration of Ni as Sulphide Phase in Sediment and in Water of a Mountain Catchment with Serpentinite Bedrock. *J. Geochem. Explor.* **2018**, *190*, 58–68. [CrossRef]
28. Igathinathane, C.; Pordesimo, L.O.; Columbus, E.P.; Batchelor, W.D.; Methuku, S.R. Shape Identification and Particles Size Distribution from Basic Shape Parameters Using ImageJ. *Comput. Electron. Agric.* **2008**, *63*, 168–182. [CrossRef]
29. Schneider, C.A.; Rasband, W.S.; Eliceiri, K.W. NIH Image to ImageJ: 25 Years of Image Analysis. *Nat. Methods* **2012**, *9*, 671–675. [CrossRef] [PubMed]
30. Bankole, S.A.; Buckman, J.; Stow, D.; Lever, H. Grain-Size Analysis of Mudrocks: A New Semi-Automated Method from SEM Images. *J. Pet. Sci. Eng.* **2019**, *174*, 244–256. [CrossRef]

31. Mathias Kondolf, G.; Lisle, T.E. Measuring Bed Sediment. In *Tools in Fluvial Geomorphology*; John Wiley & Sons, Ltd.: Hoboken, NJ, USA, 2016; pp. 278–305, ISBN 978-1-118-64855-1.
32. *EN ISO 14688-1:2018*; Geotechnical Investigation and Testing—Identification and Classification of Soil—Part 1: Identification and Description. Comité Européen de Normalisation: Brussels, Belgium, 2018.
33. Jayarathne, A.; Wijesiri, B.; Egodawatta, P.; Ayoko, G.A.; Goonetilleke, A. Role of Adsorption Behavior on Metal Build-up in Urban Road Dust. *J. Environ. Sci.* **2019**, *83*, 85–95. [CrossRef]
34. Liu, A.; Duodu, G.O.; Goonetilleke, A.; Ayoko, G.A. Influence of Land Use Configurations on River Sediment Pollution. *Environ. Pollut.* **2017**, *229*, 639–646. [CrossRef] [PubMed]
35. Strom, D.; Simpson, S.L.; Batley, G.E.; Jolley, D.F. The Influence of Sediment Particle Size and Organic Carbon on Toxicity of Copper to Benthic Invertebrates in Oxic/Suboxic Surface Sediments. *Environ. Toxicol. Chem.* **2011**, *30*, 1599–1610. [CrossRef]
36. Zhang, C.; Yu, Z.; Zeng, G.; Jiang, M.; Yang, Z.; Cui, F.; Zhu, M.; Shen, L.; Hu, L. Effects of Sediment Geochemical Properties on Heavy Metal Bioavailability. *Environ. Int.* **2014**, *73*, 270–281. [CrossRef]
37. Zhang, G.; Bai, J.; Xiao, R.; Zhao, Q.; Jia, J.; Cui, B.; Liu, X. Heavy Metal Fractions and Ecological Risk Assessment in Sediments from Urban, Rural and Reclamation-Affected Rivers of the Pearl River Estuary, China. *Chemosphere* **2017**, *184*, 278–288. [CrossRef]
38. Rayment, G.E.; Lyons, D.J. *Soil Chemical Methods: Australasia*; Csiro Publishing: Clayton South, Australia, 2011; ISBN 978-0-643-06768-4.
39. U.S. Environmental Protection Agency. SW-846 Test Method 9045D: Soil and Waste pH. Available online: https://www.epa.gov/hw-sw846/sw-846-test-method-9045d-soil-and-waste-ph (accessed on 2 December 2024).
40. Fischel, M.H.H.; Clarke, C.E.; Sparks, D.L. Arsenic Sorption and Oxidation by Natural Manganese-Oxide-Enriched Soils: Reaction Kinetics Respond to Varying Environmental Conditions. *Geoderma* **2024**, *441*, 116715. [CrossRef]
41. Bradl, H.B. Adsorption of Heavy Metal Ions on Soils and Soils Constituents. *J. Colloid Interface Sci.* **2004**, *277*, 1–18. [CrossRef]
42. Miranda, L.S.; Ayoko, G.A.; Egodawatta, P.; Goonetilleke, A. Adsorption-Desorption Behavior of Heavy Metals in Aquatic Environments: Influence of Sediment, Water and Metal Ionic Properties. *J. Hazard. Mater.* **2022**, *421*, 126743. [CrossRef] [PubMed]
43. Brady, J.P.; Kinaev, I.; Goonetilleke, A.; Ayoko, G.A. Comparison of Partial Extraction Reagents for Assessing Potential Bioavailability of Heavy Metals in Sediments. *Mar. Pollut. Bull.* **2016**, *106*, 329–334. [CrossRef]
44. Miranda, L.S.; Ayoko, G.A.; Egodawatta, P.; Hu, W.-P.; Ghidan, O.; Goonetilleke, A. Physico-Chemical Properties of Sediments Governing the Bioavailability of Heavy Metals in Urban Waterways. *Sci. Total Environ.* **2021**, *763*, 142984. [CrossRef]
45. Gunawardana, C.; Egodawatta, P.; Goonetilleke, A. Adsorption and Mobility of Metals in Build-up on Road Surfaces. *Chemosphere* **2015**, *119*, 1391–1398. [CrossRef] [PubMed]
46. Revellame, E.D.; Fortela, D.L.; Sharp, W.; Hernandez, R.; Zappi, M.E. Adsorption Kinetic Modeling Using Pseudo-First Order and Pseudo-Second Order Rate Laws: A Review. *Clean. Eng. Technol.* **2020**, *1*, 100032. [CrossRef]
47. Binda, G.; Pozzi, A.; Spanu, D.; Livio, F.; Trotta, S.; Bitonte, R. Integration of Photogrammetry from Unmanned Aerial Vehicles, Field Measurements and Discrete Fracture Network Modeling to Understand Groundwater Flow in Remote Settings: Test and Comparison with Geochemical Markers in an Alpine Catchment. *Hydrogeol. J.* **2021**, *29*, 1203–1218. [CrossRef]
48. Siddiqui, S.I.; Chaudhry, S.A. Iron Oxide and Its Modified Forms as an Adsorbent for Arsenic Removal: A Comprehensive Recent Advancement. *Process Saf. Environ. Prot.* **2017**, *111*, 592–626. [CrossRef]
49. Goldberg, S.; Johnston, C.T. Mechanisms of Arsenic Adsorption on Amorphous Oxides Evaluated Using Macroscopic Measurements, Vibrational Spectroscopy, and Surface Complexation Modeling. *J. Colloid Interface Sci.* **2001**, *234*, 204–216. [CrossRef]
50. Ma, J.; Guo, H.; Lei, M.; Zhou, X.; Li, F.; Yu, T.; Wei, R.; Zhang, H.; Zhang, X.; Wu, Y. Arsenic Adsorption and Its Fractions on Aquifer Sediment: Effect of pH, Arsenic Species, and Iron/Manganese Minerals. *Water Air Soil Pollut.* **2015**, *226*, 260. [CrossRef]
51. Zhang, G.; Wu, Z.; Qiu, Q.; Wang, Y. Efficient Sorption of Arsenic on Nanostructured Fe-Cu Binary Oxides: Influence of Structure and Crystallinity. *Front. Chem.* **2022**, *9*, 840446. [CrossRef]
52. Neidhardt, H.; Winkel, L.H.E.; Kaegi, R.; Stengel, C.; Trang, P.T.K.; Lan, V.M.; Viet, P.H.; Berg, M. Insights into Arsenic Retention Dynamics of Pleistocene Aquifer Sediments by in Situ Sorption Experiments. *Water Res.* **2018**, *129*, 123–132. [CrossRef] [PubMed]
53. Buyang, S.; Yi, Q.; Cui, H.; Wan, K.; Zhang, S. Distribution and Adsorption of Metals on Different Particle Size Fractions of Sediments in a Hydrodynamically Disturbed Canal. *Sci. Total Environ.* **2019**, *670*, 654–661. [CrossRef] [PubMed]
54. Keshavarzifard, M.; Moore, F.; Sharifi, R. The Influence of Physicochemical Parameters on Bioavailability and Bioaccessibility of Heavy Metals in Sediments of the Intertidal Zone of Asaluyeh Region, Persian Gulf, Iran. *Geochemistry* **2019**, *79*, 178–187. [CrossRef]
55. Schacht, L.; Ginder-Vogel, M. Arsenite Depletion by Manganese Oxides: A Case Study on the Limitations of Observed First Order Rate Constants. *Soil Syst.* **2018**, *2*, 39. [CrossRef]
56. Aftabtalab, A.; Rinklebe, J.; Shaheen, S.M.; Niazi, N.K.; Moreno-Jiménez, E.; Schaller, J.; Knorr, K.-H. Review on the Interactions of Arsenic, Iron (Oxy)(Hydr)Oxides, and Dissolved Organic Matter in Soils, Sediments, and Groundwater in a Ternary System. *Chemosphere* **2022**, *286*, 131790. [CrossRef]

57. Abu-Ali, L.; Yoon, H.; Reid, M.C. Effects of Organic Sulfur and Arsenite/Dissolved Organic Matter Ratios on Arsenite Complexation with Dissolved Organic Matter. *Chemosphere* **2022**, *302*, 134770. [CrossRef] [PubMed]
58. Binda, G.; Pozzi, A.; Michetti, A.M.; Noble, P.J.; Rosen, M.R. Towards the Understanding of Hydrogeochemical Seismic Responses in Karst Aquifers: A Retrospective Meta-Analysis Focused on the Apennines (Italy). *Minerals* **2020**, *10*, 1058. [CrossRef]